CrystEngComm

Accepted Manuscript

ROYAL SOCIETY OF CHEMISTRY

www.rsc.org/crystengcomm

Journal Name

RSCPublishing

ARTICLE

Formation mechanism of magnetic-plasmonic Ag@FeCo@Ag core-shell-shell nanoparticles: Fact is more interesting than fiction

Cite this: DOI: 10.1039/xoxxoooooox

Received ooth January 2012,
Accepted ooth January 2012

DOI: 10.1039/xoxxoooooox

www.rsc.org/

Mari Takahashi, Koichi Higashimine, Priyank Mohan, Derrick M. Mott, Shinya Maenosono

Combining different properties derived from different materials into a single nanoparticle allows diverse applications in many fields. In terms of plasmonic and magnetic properties, Ag and FeCo are the best candidates due to their optimal physical properties – Ag has the highest scattering cross-section of all plasmonic materials and FeCo has the highest saturation magnetization of all magnetic materials. Recently we succeeded in synthesizing magnetic-plasmonic hybrid Ag@FeCo@Ag core-shell-shell nanoparticles, however the formation mechanism of the hybrid nanoparticles was still unclear. In this study we investigated the formation mechanism of the Ag@FeCo@Ag double shell nanoparticles. Understanding the formation mechanism will help to tune the physical properties of the Ag@FeCo@Ag nanoparticles and to design novel heterostructured nanoparticles.

Introduction

Recently, multi-functional nanoparticles (NPs) have gathered attention in many fields because they show unique properties derived from each of the component materials; for example a plasmonic material, a magnetic material and a semiconductor can be incorporated into a single NP. There are several types of multi-functional NPs in which magnetic and plasmonic materials are combined. Fan and coworkers reported Fe_3O_4@Au core-shell NPs for magnetic separation of cancer cells and hyperthermia.[1] Wang *et al.* synthesized Fe_3O_4@C-Ag hybrid NPs for cellular imaging and as reusable catalysts.[2] Recently we developed Ag@FeCo@Ag core-shell-shell NPs for magnetic separation of intracellular vesicles with real-time plasmonic imaging.[3] The great features of the Ag@FeCo@Ag NPs arise from the combination of Ag and FeCo – this is because Ag has the highest scattering cross-section of all plasmonic materials[4] and FeCo has the highest saturation magnetization of all magnetic materials.[5] By taking advantage of both materials (Ag and FeCo) the Ag@FeCo@Ag NPs show extreme performance in magnetic separation and plasmonic imaging as magnetic probes and, thus, are expected to enable us to separate intracellular vesicles. There are only a few reports regarding Ag-FeCo hybrid NPs; for example Sachan *et al.* reported Ag-FeCo heterostructured NPs synthesized by the pulsed laser dewetting method.[6] Therefore, to the best of our knowledge, the chemical synthesis of Ag-FeCo hybrid NPs (*i.e.* Ag@FeCo@Ag NPs) was first achieved by our group.

The formation mechanism of multi-component core-shell NPs is not as simple as the single component NPs. There are several parameters, such as difference in reduction potentials of precursors, lattice match between components, etc., which can have significant impact on the formation of the NPs. For example, FeCo is easy to oxidize and, once oxidized, the lattice constant increases; this prevents epitaxial growth of the Ag shell on the oxidized FeCo NPs due to the large lattice mismatch. In fact, it was quite difficult when we tried to synthesize FeCo@Ag core-shell NPs because the FeCo core oxidized easily.[3] On the other the hand, reverse structures, *i.e.* Ag@FeCo core-shell NPs, could be synthesized easily, presumably because Ag is less susceptible to oxidation than FeCo. Moreover, the Ag@FeCo core-shell structure is found to have an additional benefit: suppression of oxidation of the FeCo shell due to electron transfer from the Ag core to the FeCo shell.[3] Thus it enables us to deposit another Ag shell onto the FeCo shell to form Ag@FeCo@Ag double shell NPs.[3] The second Ag shell may suppress oxidation of the FeCo shell further and, thus, Ag@FeCo@Ag double shell NPs possess higher chemical stability than Ag@FeCo core-shell NPs making them promising magnetic-plasmonic multi-functional bioprobes.

However, the formation mechanism of Ag@FeCo@Ag double shell NPs remained unclear. It is indispensable to understand their formation mechanism in order to further improve their properties and develop similar but different types of core-shell NPs. In this study we investigated the formation mechanism of Ag@FeCo@Ag NPs by comparing several different derivative NPs such as Ag@FeCo, Ag@Co, Ag@Fe and FeCo NPs. These NPs were characterized, focusing on their size, size distribution, morphology and nanostructure. Then, combining all the results, the formation mechanism of Ag@FeCo@Ag NPs is discussed.

Experimental

Chemicals

Cobalt(II) acetylacetonate [$Co(acac)_2$, purity 97%], iron(III) acetylacetonate [$Fe(acac)_3$, purity ≥99.9%], silver nitrate ($AgNO_3$, purity ≥99.9999%), 1,2-hexadecanediol (HDD, purity 90%), oleylamine (OLA, purity 70%), oleic acid (OA, purity 90%), and tetraethylene glycol (TEG, purity 99%) were purchased from Sigma-Aldrich and used as received. Hexane was purchased from Nacalai Tesque. Acetone was purchased from Kanto Chemical, and toluene was purchased from Wako Pure Chemical.

Synthesis of Ag@FeCo@Ag NPs

Synthesis of Ag@FeCo@Ag NPs by combination of a hot injection method and a polyol method was followed, as previously reported.[3] The synthetic procedure and temperature profile are shown schematically in Fig. 1. First 0.1 mmol of $AgNO_3$, 1.0 mmol of HDD, 10 mmol of OLA, 8 mmol of OA and 10 mL of TEG were added into a three-neck flask. The reaction solution was vigorously stirred at room temperature for 5 min with Ar bubbling, then the temperature was increased to 100 ºC for 10 min to remove volatile substances. After 10 min the solution temperature was increased to 170 ºC at which point the first stock solution containing 0.2 mmol of $Co(acac)_2$, 0.2 mmol of $Fe(acac)_3$, 1 mL of OLA and 2 mL of toluene was injected, keeping the temperature constant. Subsequently the temperature was increased to 250 ºC and the second stock solution containing 0.1 mmol of $AgNO_3$, 1 mL of OLA and 1 mL of toluene were injected. Then the temperature was decreased to 230 ºC for 10 min. After the reaction the solution was cooled down and washed with acetone and hexane following a previously described routine.[3] The final NPs were dried under vacuum.

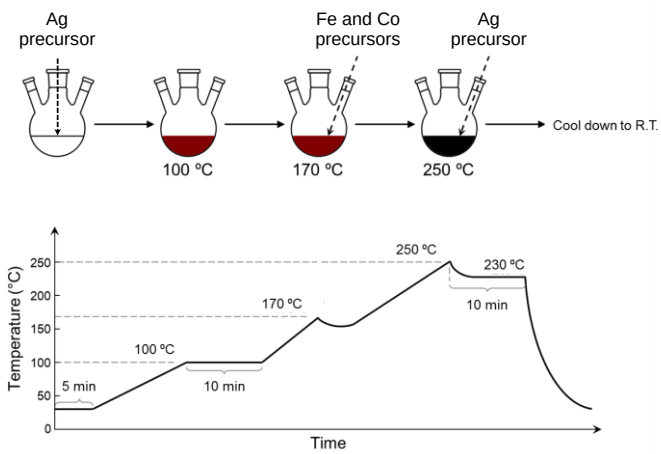

Fig. 1 Synthetic procedure and temperature profile for synthesis of Ag@FeCo@Ag NPs.

Synthesis of Ag@FeCo NPs

The same synthetic procedure as described for the synthesis of Ag@FeCo@Ag NPs was followed for the synthesis of Ag@FeCo NPs. The only difference was that, when the temperature reached 250 ºC, a small amount of the NPs was sampled and the temperature reduced to 230 ºC without injecting the second Ag stock solution. The rest of the process, including the washing process, was identical to the synthesis of Ag@FeCo@Ag NPs.

Synthesis of FeCo NPs without Ag precursor

Synthesis of FeCo NPs followed a previous report,[3] with samples of the reaction mixture removed at various points. First 0.2 mmol of $Co(acac)_2$, 0.2 mmol of $Fe(acac)_3$, 1.0 mmol of HDD, 10 mmol of OLA, 8 mmol of OA and 10 mL of TEG were added into a three-neck flask. Then the same procedure used for the previous samples was followed until the volatile substances were removed. The temperature was increased to 290 ºC with sampling at 230, 250, 270 and 290 ºC. Then the temperature was kept at 290 ºC for 20 min. After the reaction the solution was allowed to cool naturally and the supernatant was transferred into two tubes. Following this the samples were diluted with acetone to 45 mL total volume. The tubes were left unagitated for 2 hours to precipitate the NPs naturally. Then the tubes were centrifuged at 4500 rpm for 5 min. After discarding the supernatant the NPs were dried in a vacuum drying system.

Synthesis of Ag@Co and Ag@Fe NPs

Ag@Co and Ag@Fe core-shell NPs were synthesized following the same protocol as the Ag@FeCo NPs. The only difference was the contents of the stock solution which was injected at 170 ºC. In the case of the Ag@Co NP synthesis the stock solution did not contain $Fe(acac)_3$ and in the case of Ag@Fe NPs the stock solution did not contain $Co(acac)_2$. In both cases, after the injection of the stock solution, the temperature was increased to 250 ºC. When the temperature reached 250 ºC the temperature was decreased to 230 ºC for 10 min. These NPs were washed with acetone and hexane in a manner similar to the case of Ag@FeCo@Ag NPs.

Characterization of the NPs

The NPs were characterized by transmission electron microscopy (TEM), a scanning TEM (STEM) equipped with a high-angle annular dark-field (HAADF) detector, energy-dispersive X-ray spectroscopy (EDS) elemental mapping and X-ray diffraction (XRD). TEM analysis was performed on a Hitachi H-7650 microscope operated at 100 kV. STEM-HAADF imaging and EDS elemental mapping were performed on a JEOL JEM-ARM200F microscope operated at 200 kV with a spherical aberration corrector, and a nominal resolution of 0.8 Å. XRD patterns were collected on an X-ray diffractometer (Rigaku MiniFlex600) operated in reflection geometry at room temperature with Cu Kα radiation (1.5418 Å).

Results

Ag@FeCo and Ag@FeCo@Ag NPs

Fig. 2a-d shows TEM, STEM-HAADF and low and high magnification EDS elemental mapping images of Ag@FeCo core-shell NPs. Based on the TEM images the average diameter of the Ag@FeCo NPs was found to be 16.9±3.4 nm (n=855). Contrast

variations in the STEM-HAADF image indicate differences in atomic number (the brightness is approximately proportional to the square of the atomic number, Z^2). It was found that the Ag@FeCo NPs have a core-shell structure, and that the cores consist of heavier elements than the shells. Fig. 2c shows that several of the Ag@FeCo NPs investigated have a large Ag core and a partial FeCo shell. In Fig. 2d it can be seen that the FeCo shell has a composition gradient: becoming Co rich nearer the core and Fe rich nearer the outer surface. This observation was supported by line profiles, as shown in Fig. 2e. The line profile was taken along the yellow line indicated in Fig. 2d.

Fig. 2f-i shows a TEM image, a STEM-HAADF image and EDS elemental mapping images of Ag@FeCo@Ag double shell NPs. Based on analysis of the TEM images the average diameter of the Ag@FeCo@Ag NPs was found to be 13.5±2.5 nm (n=531). Because the mean size of the Ag cores in Ag@FeCo@Ag NPs was estimated to be 9.5 nm,[3] the average thickness of FeCo shell was calculated to be ca. 2.1 nm. Based on XRD analysis for Ag@FeCo@Ag NPs, the mean crystalline sizes of Ag and FeCo were determined to be 3.3 and 1.6 nm, respectively.[3] These results suggest that both Ag core and FeCo shell have relatively poor crystallinity. Fig. 2j shows an EDS line profile of an Ag@FeCo@Ag NP taken along the yellow line indicated in Fig. 2i. Compared to the line profile of the Ag@FeCo NP (Fig. 2e), it is obvious that the outer Ag shell was formed (although we are not ruling out the possibility that the outer shell consists of FeCoAg ternary alloy). Interestingly the mean diameter of the Ag@FeCo NPs was significantly greater than that of the Ag@FeCo@Ag NPs. According to the EDS elemental mapping of Ag@FeCo NPs (Fig. 2c), the reason for the Ag@FeCo NPs' large size may be attributed to the large Ag cores.

The size distributions of Ag@FeCo NPs sampled immediately after the temperature reached 250 ºC, of which the mean diameter is 6.4±1.8 nm (n=529) (see ESI, Fig. S1a), Ag@FeCo NPs and Ag@FeCo@Ag NPs are shown in Fig. 3. The size distribution of Ag@FeCo NPs is also greater than that of Ag@FeCo@Ag NPs. This is mainly due to the presence of the large Ag cores in the case of Ag@FeCo NPs.

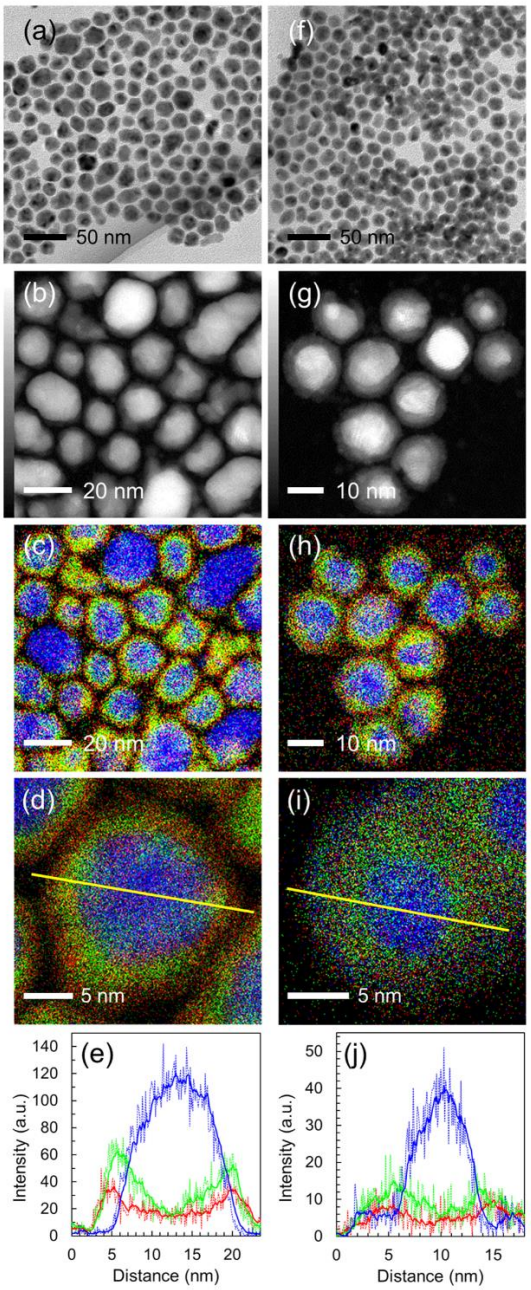

Fig. 2 (a) TEM image, (b) STEM-HAADF image and (c) low magnification EDS elemental mapping image of Ag@FeCo NPs and (d) high magnification EDS elemental mapping image of a single Ag@FeCo NP. (e) The line profile of the yellow line indicated in (d). Blue, red and green lines correspond to Ag L edge, Fe K edge and Co K edge, respectively. (f) TEM image, (g) STEM-HAADF image, (h) low magnification EDS elemental mapping image of Ag@FeCo@Ag NPs and (i) EDS elemental mapping image of a single Ag@FeCo@Ag NP. (j) The line profile of the yellow line indicated in (i). Blue, red and green lines correspond to Ag L edge, Fe K edge and Co K edge, respectively.

FeCo NPs

Based on the TEM analysis almost no NPs were formed when the temperature was below 270 ºC, however NPs were found to be formed when the temperature reached 290 ºC. The size of the NPs sampled immediately after the temperature reached 290 ºC was 4.9±1.1 nm (n=149) (see ESI, Fig. S1b). After the completion of the reaction, the size of the NPs increased to 8.3±1.5 nm (n=165) (see ESI, Fig. S1c). Fig. 4a shows the size distribution of FeCo NPs sampled immediately after the temperature reached 290 ºC and FeCo NPs after the completion of the reaction. Fig. 4b shows the XRD pattern of the FeCo NPs after the completion of the reaction. It clearly indicates that those NPs are not the FeCo phase but the wüstite-like $Co_xFe_{1-x}O$ phase[7] as reported previously.[3]

Ag@Co NPs and Ag@Fe NPs

Fig. 5a-c shows representative TEM, STEM-HAADF and EDS elemental mapping images of the Ag@Co NPs. The diameter of

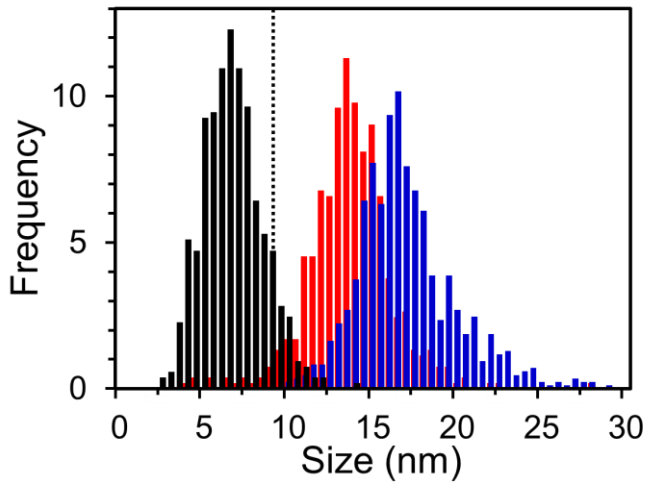

Fig. 3 Size distribution of NPs. Black, blue and red histograms correspond to Ag@FeCo core-shell NPs sampled immediately after the temperature reached 250 ºC, Ag@FeCo core-shell NPs (final product) and Ag@FeCo@Ag double shell NPs, respectively. In all the cases, the total number of NPs was normalized to 100. Dashed line indicates the average size of the Ag cores of Ag@FeCo@Ag NPs (9.3 nm).

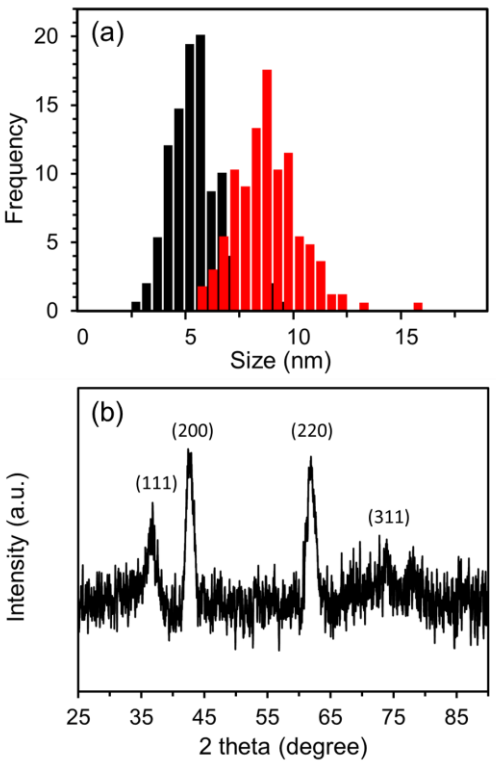

Fig. 4 (a) Size distribution of FeCo NPs. Black and red histograms correspond to FeCo NPs sampled immediately after the temperature reached 290 ºC and FeCo NPs after the completion of the reaction, respectively. In both cases the total number of the NPs was normalized to 100. (b) XRD pattern of FeCo NPs (final product) indicating that they have the wüstite-like $Co_xFe_{1-x}O$ phase.

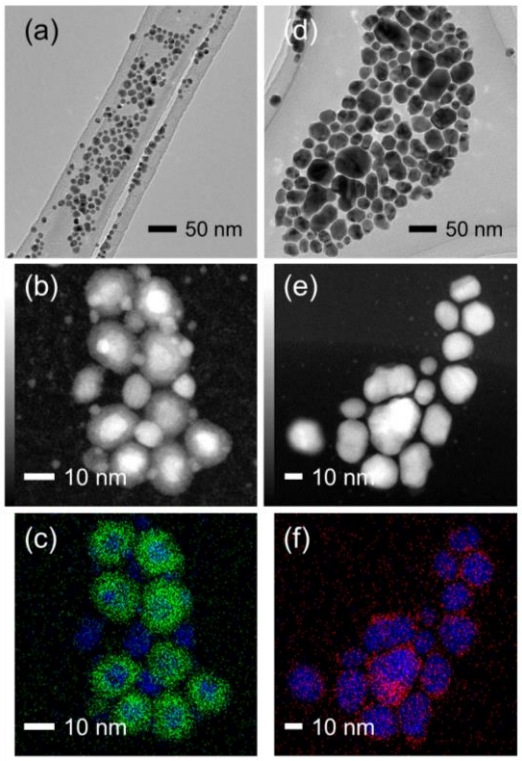

Fig. 5. (a) TEM image, (b) STEM-HAADF image and (c) EDS elemental mapping image of Ag@Co core-shell NPs. (d) TEM image, (e) STEM-HAADF image and (f) EDS elemental mapping image of Ag@Fe core-shell NPs. Blue, green and red colours represent Ag L edge, Co K edge and Fe K edge, respectively.

the Ag@Co NPs was 13.8±3.5 nm (n=230) based on the TEM analysis. The distinct core-shell structure was confirmed for the majority of the particles, even though some uncoated Ag seeds remained in the system. Fig. 5d-f shows representative TEM, STEM-HAADF and EDS elemental mapping images of the Ag@Fe NPs. The Fe shell was found not to be uniformly formed. Only a thin and non-uniform Fe shell was formed around the Ag core as seen in Fig. 5f. The diameter of the Ag@Fe NPs was 30.4±8.6 nm (n=164) based on the TEM analysis. The reason for the large size was attributed to the large Ag cores.

Discussion

Ag cores and their catalytic activity

To begin with let's consider the results of FeCo NPs synthesized in the absence of Ag precursor. As mentioned above, almost no NP was formed when the temperature was below 270 °C. As shown in Fig. 4 only small $Co_xFe_{1-x}O$ NPs (4.9 nm) were formed when the reaction temperature was raised to 290 °C; yet the FeCo shell was successfully formed during the synthesis of Ag@FeCo NPs and Ag@FeCo@Ag NPs (Fig. 2) even at the reduced reaction temperature (< 250 ºC). These results indicate it is highly possible that the Ag core acts as a catalyst for the reduction of Fe and Co. Therefore we will consider the catalytic action of the Ag cores in depth. The average diameter of NPs sampled at 250 °C during the

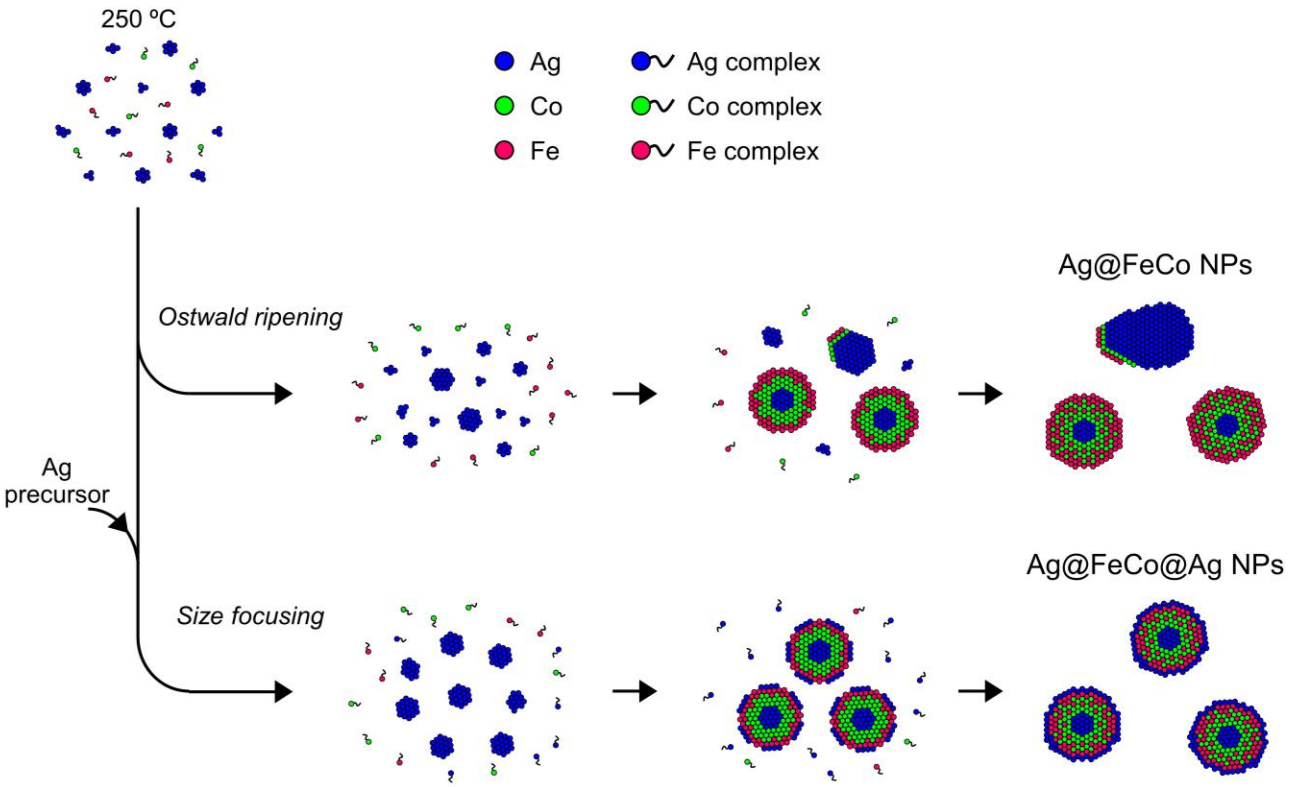

Fig. 6 Illustration of the formation mechanisms of Ag@FeCo, Ag@FeCo@Ag, Ag@Co and Ag@Fe NPs. The blue, green and red circles represent Ag, Co and Fe atoms, respectively.

synthesis of Ag@FeCo NPs was 6.4±1.8 nm, as mentioned earlier. Comparing the size of the sampled NPs with the average sizes of the Ag cores in the STEM-HAADF and EDS elemental mapping images of Ag@FeCo NPs and Ag@FeCo@Ag NPs (11.8±1.5 and 9.3±2.5 nm, respectively), the sampled NPs seem to be Ag NPs because the galvanic etching of Ag cores by Fe and/or Co cations is unlikely. This means the Ag cores had not been covered with FeCo shell, even when the reaction temperature reached 250 ºC. Note that the mean size and size distribution of the Ag cores of Ag@FeCo@Ag NPs were estimated from several different samples synthesized under the same conditions, while those values of Ag cores of Ag@FeCo NPs were estimated from one sample, excluding the NPs that had a large Ag core and only a partial FeCo shell. For this reason, the standard deviation in the case of the Ag@FeCo@Ag NPs is a bit larger than that in the case of the Ag@FeCo NPs. This result suggests that the size of the Ag cores, in both Ag@FeCo NPs which have a complete FeCo shell and Ag@FeCo@Ag NPs, are statistically identical. Why did the reduction of Fe and Co take place after the temperature reached 250 ºC, even though both metal precursors were injected at 170 ºC?

It is well known that Ag NPs have size dependant catalytic activity.[8] Specifically the Ag NPs of appropriate size are catalytically active for reduction reactions *via* working as a bridge to enhance the electron transfer from reductant to precursor.[8] In our system it can be thought that TEG acts as the main electron donor to the Ag NPs and the Co or Fe complex acts as an acceptor of electrons from the Ag NPs. These redox reactions depend on the electrochemical standard potential – this changes with the Ag core size. Therefore it is only when the Ag core is an appropriate size to act as an intermediate between electron donors and acceptors that the Ag NPs can show catalytic activity. In our case, it is approximately 10 nm, because the size of the Ag cores in both Ag@FeCo NPs which have a complete FeCo shell and Ag@FeCo@Ag NPs eventually settled around this value.

Formation mechanism of Ag@FeCo NPs

As can be seen in Fig. 2c, there were two types of Ag@FeCo NPs: Ag@FeCo NPs which have a complete FeCo shell and Ag@FeCo NPs which have a large Ag core and partial FeCo shell. The large Ag cores were not observed in the Ag@FeCo@Ag NPs even though we scanned several different fields of view as shown in Fig. 2h. As mentioned above, the average diameter of the Ag cores of the Ag@FeCo NPs which have a complete FeCo shell and the Ag@FeCo@Ag NPs was approximately 10 nm. On the other hand, the size of Ag cores of the Ag@FeCo NPs which have a large Ag core and partial FeCo shell was found to be 22.6±2.4 nm, raising the overall average diameter of Ag@FeCo NPs.

If we don't inject the second Ag stock solution at 250 ºC (as in the case of Ag@FeCo NPs) both the average size and the size

distribution of the Ag cores become larger through the Ostwald ripening. Then the Ag cores whose size reaches the critical size, $D_c \approx 10$ nm (at which point they can act as intermediates for electron transfer from polyol to Co and Fe complexes), start to act as reducing catalysts for the reduction of Co and Fe. However, because the reduction potential of Co^{2+}/Co (–0.28 V versus SHE) is higher than Fe^{2+}/Fe (–0.45 V versus SHE), Co is reduced before Fe. It is known that bulk Ag and Co do not form an alloy,[9] therefore Co atoms do not diffuse into the Ag core. Fe also does not form an alloy with Ag,[10] but can form an alloy with Co in the bulk.[11] Because Fe forms an alloy with Co easily, when Fe is reduced onto the Co shell it diffuses into the Co shell to make an alloy. Therefore, as shown in Fig. 2, the FeCo shell was Co rich around the Ag core. The Ag@FeCo NPs which have a complete FeCo shell were formed in this way. EDS elemental mapping images of Ag@Co NPs and Ag@Fe NPs (Fig. 5) also indicate that Co could be reduced earlier resulting in a thicker shell than Fe.

On the other hand, Ag cores smaller than D_c still remained when FeCo shells were formed on the Ag cores larger than D_c. Those small Ag cores couldn't be covered with Co and Fe because they didn't have catalytic activity, and thus they continued to undergo the Ostwald ripening. In the meantime, Ag cores larger than D_c were completely covered with FeCo shell. At that point, the Ag precursor was running out. In addition little Co and Fe precursor remained, because they were already incorporated into the Ag@FeCo NPs with a complete FeCo shell. Therefore, in the case of the Ag@FeCo NPs which have a large Ag core and partial FeCo shell, it is likely that their Ag cores reached D_c very late. Thus only a thin and partial Co shell could be formed onto the Ag cores, and the Ag cores continued to grow in the uncovered areas *via* Ostwald ripening. Thus the Ag@FeCo NPs with large Ag cores were formed. Note that the shape of the large Ag cores is not spherical because one side was partially covered by the FeCo shell, as shown in Fig. 2c. An illustration of the proposed formation mechanism is shown in Fig. 6.

Formation mechanism of Ag@Co and Ag@Fe NPs

In the case of formation of Ag@Co NPs, Co complexes started to reduce when the Ag cores, which were undergoing Ostwald ripening, reached D_c. The Ag cores, which grew up later, could not be covered by the Co shell because most of the Co was already reduced into the existing Co shells. Note that, in the case of the synthesis of Ag@FeCo NPs and Ag@FeCo@Ag NPs, the amount of precursor for the FeCo shell was 0.4 mmol in total while, in the case of the Ag@Co NPs, the precursor amount for the Co shell was 0.2 mmol. Finally, in the case of the Ag@Fe NPs, because the Fe complexes were hardly reduced, and the Ostwald ripening of Ag cores continued, a small amount of Fe complex was reduced onto the Ag cores, resulting in a partial Fe shell. We are not sure whether the critical size of the Ag core, at which it can facilitate electron transfer from polyol to Fe complexes, is larger than the critical size for reduction of Co complexes, but this is possible.

Formation mechanism of Ag@FeCo@Ag NPs

Based on the formation mechanism of Ag@FeCo NPs described above, the formation mechanism of Ag@FeCo@Ag NPs will be discussed. In the synthesis of Ag@FeCo@Ag NPs a second Ag precursor was injected at 250 ºC, causing size focusing[12] of the Ag cores. This means that the Ag cores were growing while the size distribution was decreasing. Then most of the Ag cores simultaneously reached the critical size, followed by uniform FeCo shell formation; that is, monodispersed Ag@FeCo seed NPs were successfully formed in the reaction solution. In fact, the average thickness of FeCo shell in the case of Ag@FeCo@Ag NPs (ca. 2.1 nm) was found to be smaller than that of Ag@FeCo core-shell NPs which have a complete FeCo shell (ca. 2.5 nm), because Fe and Co precursors were distributed to all Ag cores equally. At that point, the amount of remaining Ag precursor was not enough to newly nucleate Ag NPs, and thus the FeCo shell was formed first. In other words, when the size of the Ag cores reached D_c, the FeCo shell started to form on the Ag cores – interrupting the further growth of the Ag cores (Fig. 6). Since the Ag precursor remained in the reaction solution, and the reduction potential of Ag^+/Ag (0.8 V versus SHE) is higher than Co^{2+}/Co and Fe^{2+}/Fe, Ag would continue to be reduced during the formation of the FeCo shell. If this is the case, how does the outer Ag shell form?

One possible explanation is surface segregation, which is a well-known phenomenon in various alloy systems; in this case one of the alloy components may enrich the surface region. One can evaluate whether surface segregation will take place in a particular alloy system of interest by assessing the surface segregation energy, E_{segr}, which is given by taking the difference in the surface energies of the impurity and the host. Ruban and coworkers calculated E_{segr} of single transition metal impurities in transition-metal hosts using a Green's-function linear-muffin-tin-orbitals method.[13] According to their calculation, E_{segr} is –2.37 eV for an Ag impurity atom at the bcc Fe surface and –0.93 eV for an Ag atom at the hcp Co surface.[13] This means that the surface segregation of Ag is energetically favourable, and will take place spontaneously when Ag atoms are incorporated in an FeCo shell.

Based on the considerations above, the important period in which the FeCo shell and Ag outer shell were formed is after the temperature reaches 250 ºC. This means that, even if all the precursors (Ag, Fe and Co) are put in the flask from the very beginning and another Ag precursor is injected at 250 ºC, the same structure as the Ag@FeCo@Ag NPs should be obtained. Additionally, if all the precursors (Ag, Fe and Co) are injected into the flask at 170 ºC and another Ag precursor is injected at 250 ºC the Ag@FeCo@Ag NP structure should be obtained again. In fact, we carried out those syntheses and succeeded in obtaining almost the same structure as the Ag@FeCo@Ag NPs (see ESI, Fig. S2).

Towards improvements of the NP properties

We have already reported that the saturation magnetization, M_s, of the FeCo shell in the Ag@FeCo@Ag NPs was much lower than the M_s of the bulk counterpart (FeCo bulk crystal).[3] There are several possible causes for the reduction of M_s: (1) a magnetically dead surface layer, (2) surface oxidation, (3) the composition gradient and (4) poor crystallinity. To improve M_s more considerably than the present Ag@FeCo@Ag NPs, two approaches come quickly to mind. Firstly, make the FeCo shell more homogeneous, avoiding generation of the compositional

gradient in the shell, because it is known that $Fe_{60}Co_{40}$ exhibits higher M_s than either pure Fe or pure Co.[14] Secondly, make the Ag outer shell thicker to suppress the surface oxidation of the FeCo shell more effectively. This is not that simple because the Ag outer shell is thought to be formed through the surface segregation of Ag atoms incorporated in the FeCo shell during the reaction. Based on our findings in the present study these attempts are under investigation.

Conclusion

The formation mechanism of Ag@FeCo@Ag NPs is elucidated. It was thought that FeCo and Ag shells might be formed on Ag cores sequentially when we designed the synthesis scheme, so that Fe and Co precursors were simultaneously injected at 170 ºC followed by the injection of another Ag precursor at 250 ºC. However, the fact is more attractive than anticipated. Both Fe and Co precursors had not been reduced yet when the temperature reached 250 ºC, even though they were injected well before the injection of Ag precursor. This is presumably because the size of the Ag cores was not large enough to act as a catalyst for the reduction of Fe and Co before the injection of another Ag precursor. After the injection of Ag precursor at 250 ºC, the Ag cores quickly grow to reach the critical size at which point they can act as intermediates for electron transfer from polyol to Co and Fe complexes. In addition, the size focusing phenomenon took place during the crystal growth of the Ag cores, and thus most of the Ag cores could possess catalytic activity all together. Then, the reduction of Co took place first on the Ag cores, followed by the reduction of Fe. As a result, the FeCo shell with composition gradient (Co rich near the interface between Ag core and FeCo shell and Fe rich at the outer surface) was formed. During the formation of the FeCo shell, Ag precursor still remained in the solution. Therefore, a small amount of Ag atoms were incorporated into the FeCo shell. However, because Ag is immiscible to Co and Fe, surface segregation of the Ag took place to form the Ag outer shell. The knowledge obtained from the present study is not only informative for improving the properties of the Ag@FeCo@Ag NPs, but also helpful for designing novel heterostructured NPs.

Acknowledgements

This work was supported by a Grant-in-Aid for Scientific Research, Grant Number 26600053 (SM). We thank Ian Godfrey for proofreading the manuscript.

Notes and references

School of Materials Science, Japan Advanced Institute of Science and Technology, 1-1 Asahidai, Nomi, Ishikawa 923-1292, Japan.

† Electronic Supplementary Information (ESI) available: TEM images of Ag@FeCo NPs sampled at 250 ºC, $Co_xFe_{1-x}O$ NPs sampled at 290 ºC, and $Co_xFe_{1-x}O$ NPs after the reaction, and TEM, STEM-HAADF and EDS elemental mapping images of Ag@FeCo@Ag NPs synthesized under different synthetic conditions. See DOI: 10.1039/b000000x/

1 Z. Fan, M. Shelton, A. K. Singh, D. Senapati, S. A. Khan and P. C. Ray, *ACS Nano*, 2012, **6**, 1065.
2 H. Wang, J. Shen, Y. Li, Z. Wei, G. Cao, Z. Gai, K. Hong, P. Banerjee and S. Zhou, *ACS Appl. Mater. Interfaces*, 2013, **5**, 9446.
3 M. Takahashi, P. Mohan, A. Nakade, K. Higashimine, D. Mott, T. Hamada, K. Matsumura, T. Taguchi and S. Maenosono, *Langmuir*, 2015, **31**, 2228.
4 K. Aslan, J. R. Lakowicz and C. D. Geddes, *Curr. Opin. Chem. Biol*., 2005, **9**, 538.
5 S. Maenosono and S. Saita, *IEEE Trans. Magn*. 2006, **42**, 1638.
6 R. Sachan, A. Malasi, J. Ge, S. Yadavali, H. Krishna, A. Gangopadhyay, H. Garcia, G. Duscher and R. Kalyanaraman, *ACS Nano*, 2014, **8**, 9790.
7 W. Baaziz, B. P. Pichon, Y. Liu, J. M. Grenèche, C. Ulhaq-Bouillet, E. Terrier, N. Bergeard, V. Halté, C. Boeglin, F, Choueikani, M. Toumi, T. Mhiri and S. Begin-Colin, *Chem. Mater*., 2014, **26**, 5063.
8 N. R. Jana, T. K. Sau and T. Pal, *J. Phys. Chem. B*, 1999, **103**, 115.
9 I. Karakaya and W. T. Thompson, *Bull. Alloy Phase Diagrams*, 1986, **7**, 259.
10 L. J. Swartzendruber, *Bull. Alloy Phase Diagrams*, 1984, **5**, 560.
11 H. Okamoto, *J. Phase Equilib. Diffus*., 2008, **29**, 383.
12 X. Peng, J. Wickham and A. P. Alivisatos, *J. Am. Chem. Soc*., 1998, **120**, 5343.
13 A. V. Ruban, H. L. Skriver and J. K. Nørskov, *Phys. Rev. B*, 1999, **59**, 15990.
14 M. Abbas, Md. N. Islam, B. P. Rao, T. Ogawa, M. Takahashi and C. G. Kim, *Mater. Lett*., 2013, **91**, 326.

The formation mechanism of Ag@FeCo@Ag core-shell-shell nanoparticles (NPs) which are synthesized by combination of a multi-step hot injection method and a polyol method was investigated by comparing several different derivative NPs such as Ag@FeCo, Ag@Co, Ag@Fe and FeCo NPs.